

1

Supporting Information

3

4 Near-Unity Room Temperature Phosphorescent Quantum Yield Induced by Halogen-Halogen 5 Interaction in Chiral Hybrid Copper(I) Iodine Clusters

6

7 Yanjing Qin,^{† [a]} Jianwu Wei,^{† [a]} Jing Li,^[a] Xianli Li,^[a] Binbin Luo,^{*[a]} Peican Chen,^[a] Liya Zhou,^[a] Jin Zhong
8 Zhang,^[b] and Oi Pang^{*[a]}

9

¹⁰*School of Chemistry and Chemical Engineering/State Key Laboratory of Featured Metal Materials and Life-cycle
11 Safety for Composite Structures/Key Laboratory of Electrochemical Energy Materials Guangxi University
12 Nanning 530004, Guangxi, P. R. China*

^b Department of Chemistry and Biochemistry, University of California, Santa Cruz, California 95064, United States

14 *Corresponding authors: bbluo@gxu.edu.cn, qipang@gxu.edu.cn

Table of Contents

Table of Contents	2
Experimental Procedures	3
<i>Material:</i>	3
<i>Synthesis of R/S-Cl and R/S-Br crystals:</i>	3
<i>Synthesis of R/S-Cl and R/S-Br powders:</i>	3
<i>Characterizations:</i>	3
Table S1.	5
Table S2.	6
Table S3.	7
Table S4.	7
Figure S1.	8
Figure S2.	8
Figure S3.	9
Figure S4.	9
Figure S5.	10
Figure S6.	10
Figure S7.	11
Figure S8.	11
Figure S9.	12
Figure S10.	12
Figure S11.	13
Figure S12.	13
Figure S13.	14
Figure S14.	14
Figure S15.	14
Figure S16.	15
Figure S17.	15
Figure S18.	16
Figure S19.	16
Figure S20.	17
Figure S21.	17
Figure S22.	18
Figure S23.	18
Figure S24.	19
Figure S25.	19
Figure S26.	20
Figure S27.	20
References.....	21

Experimental Procedures

Material:

Copper(I) iodide (CuI, 99.5%, Aladdin), potassium iodide (KI, 99%, Aladdin). (*R/S*)-4-chloro- α -methylbenzylamine (99%, Adamas), ethanol (99.5%, Keshi), (*R/S*)-4-bromo- α -methylbenzylamine (98%, Adamas), No further purification was carried out on the chemicals before use.

Synthesis of R/S-Cl and R/S-Br crystals:

The four single crystals were prepared by using the room temperature solvent slow diffusion method. In a narrow-diameter glass tube, 0.50 mmol of Cu(I) dissolved in 2.00 mL of saturated KI aqueous solution as the bottom layer, the intermediate buffer layer was selected from 1.00 mL of a 1:1 mixture of ethanol and water, and the top layer was 2.0 mL of ethanol containing 0.50 mmol of (*R/S*)-4-chloro- α -methylbenzylamine. After standing for 2-3 days, the colorless needle-like crystals are obtained. The obtained crystals are washed with large amounts of water in rapid repetitions several times. A similar method is used to synthesize the *R/S*-Br single crystal, replacing (*R/S*)-4-Chloro- α -Methylbenzylamine with (*R/S*)-4-Bromo- α -Methylbenzylamine.(pay some attention to significant figures)

Synthesis of R/S-Cl and R/S-Br powders:

25 mL of ethanol and 5.0 mmol of CuI were taken in a 50 mL beaker and stirred at room temperature, after stirring for 10 min, 1.0 mmol of (*R/S*)-4-chloro- α -methylbenzylamine or (*R/S*)-4-bromo- α -methylbenzylamine was injected quickly, immediately there is powder precipitation, continue to stir for 5 min to make the reaction fully, the obtained powder will be filtered, washed with a large amount of water for several times.

Characterizations:

Single-crystal data were collected on a Bruker D8 instrument under Mo K α radiation ($\lambda = 0.71073 \text{ \AA}$) operating at 50 kV and 30 mA. The crystal structures of the samples were visualized and analyzed using OLEX2 and VESTA software. The diffraction patterns of the samples were obtained via powder X-ray diffraction (D8 Advance, Bruker, Germany) with Cu-K α radiation ($\lambda = 0.15405 \text{ nm}$) operating at 40 kV and 30 mA, with a scanning range of 5° to 50° and a scanning rate of 12°/min. Deposition numbers 2373940 (for *R*-Cl), 2374453 (for *S*-Cl), 2373620 (for *R*-Br), and 2373939 (for *S*-Br), contain the supplementary crystallographic data for this paper. These data are provided free of charge by the

Cambridge Crystallographic Data Center and Fachinformationszentrum Karlsruhe (<http://www.ccdc.cam.ac.uk/structures>).

The microscopic morphology of single crystals was recorded with a German ZEISS Sigma 300 scanning electron microscope (SEM) at an accelerating voltage of 300 kV. The X-ray photoelectron spectroscopy (XPS) of the single crystals was obtained with Thermo Fisher Scientific K-Alpha. Thermogravimetric analysis (TGA) measurements were performed on a Rigaku simultaneous thermal analyzer.

The PL spectra, PLE spectra, and time-resolved PL of the samples were measured on an FLS1000 fluorescence spectrometer from Edinburgh Instruments. Photoluminescence quantum yield (PLQY) was determined using an FLS1000 fluorescence spectrometer with an integrating sphere accessory. The excitation and emission light emitted from the surface of the samples in all directions were homogenized by the integrating sphere, and the light at the exit end entered the monochromator for detection. The specific PLQY formula is as follows: $\Phi = E_a - E_a/La - Lc$, where Φ is the absolute PLQY, La is the total amount of excitation light, Lc is the amount of excitation light remaining after direct excitation, Ec is the amount of emitted light, and Ea is the background of the sphere. The PL quenching behavior of the samples was measured using an Oxford Optistat DN-V cryostat. The samples were analyzed by infrared spectroscopy using a Thermo Nicolet IS50 Fourier Transform Infrared Spectrometer (FTIR). The optical absorption spectra of the samples were recorded at room temperature using a solid-state UV-2600 spectrophotometer. Circular dichroism spectra were measured using an MOS-450 circular dichroism spectrometer.

The prepared crystals were encapsulated in 365 nm LEDs using epoxy resin, and then the fabricated LEDs were placed in an equipped LED spectrometer tester (HAAS 2000). The scintillation performance of the sample was evaluated by a self-constructed X-ray imaging system, with X-ray radiation from a D8 Focus diffractometer (Bruker) equipped with Cu Ka radiation ($\lambda = 0.15405$ nm), and imaging photos were captured via a high-definition digital camera.

Table S1. Crystal data and structure refinement for *R*-Cl and *S*-Cl.

Identification code	<i>R</i> -Cl	<i>S</i> -Cl
Moiety formula	C ₃₂ H ₄₀ Cl ₄ Cu ₄ I ₄ N ₄	C ₃₂ H ₄₀ Cl ₄ Cu ₄ I ₄ N ₄
Formula weight	346.06	346.06
Temperature/K	150.00	150.00
Crystal system	monoclinic	monoclinic
Space group	<i>C</i> 2	<i>C</i> 2
<i>a</i> /Å	31.1426(9)	31.1399(9)
<i>b</i> /Å	7.5708(2)	7.5678(2)
<i>c</i> /Å	18.1486(5)	18.1474(5)
$\alpha/^\circ$	90	90
$\beta/^\circ$	102.0620(10)	102.0590(10)
$\gamma/^\circ$	90	90
Volume/Å ³	4184.5(2)	4182.3(2)
<i>Z</i>	4	4
$\rho_{\text{calcd}}/\text{cm}^3$	2.197	2.198
μ/mm^{-1}	5.241	5.243
F(000)	2624.0	2624.0
Crystal size/mm ³	0.2 × 0.15 × 0.1	0.2 × 0.15 × 0.1
Radiation	MoKα ($\lambda = 0.71073$)	MoKα ($\lambda = 0.71073$)
2Θ range for data collection/°	5.364 to 52.828	3.872 to 52.842
Index ranges	-38 ≤ <i>h</i> ≤ 38, -9 ≤ <i>k</i> ≤ 9, -22 ≤ <i>l</i> ≤ 22	-38 ≤ <i>h</i> ≤ 38, -9 ≤ <i>k</i> ≤ 9, -22 ≤ <i>l</i> ≤ 22
Reflections collected	41428	41453
Independent reflections	8545 [$R_{\text{int}} = 0.0470$, $R_{\text{sigma}} = 0.0347$]	8552 [$R_{\text{int}} = 0.0482$, $R_{\text{sigma}} = 0.0352$]
Data/restraints/parameters	8545/1/437	8552/1/437
Goodness-of-fit on F ²	1.149	1.138
Final R indexes [$I \geq 2\sigma(I)$]	$R_1 = 0.0338$, $wR_2 = 0.0747$	$R_1 = 0.0340$, $wR_2 = 0.0730$
Final R indexes [all data]	$R_1 = 0.0376$, $wR_2 = 0.0767$	$R_1 = 0.0391$, $wR_2 = 0.0758$
Largest diff. peak/hole/eÅ ⁻³	0.80/-0.92	0.70/-0.92
Flack parameter	0.020(11)	0.010(11)
CCDC	2373940	2374453

Table S2. Crystal data and structure refinement for *R*-Br and *S*-Br.

Identification code	<i>R</i> -Br	<i>S</i> -Br
Moiety formula	$C_{32}H_{40}Br_4Cu_4I_4N_4$	$C_{32}H_{40}Br_4Cu_4I_4N_4$
Formula weight	390.52	390.52
Temperature/K	150.00	150.00
Crystal system	monoclinic	monoclinic
Space group	<i>C</i> 2	<i>C</i> 2
<i>a</i> /Å	19.3339(6)	19.3397(8)
<i>b</i> /Å	7.5998(2)	7.6012(3)
<i>c</i> /Å	15.8822(4)	15.8721(7)
$\alpha/^\circ$	90	90
$\beta/^\circ$	112.4050(10)	112.4210(10)
$\gamma/^\circ$	90	90
Volume/Å ³	2157.47(10)	2156.90(16)
<i>Z</i>	2	2
$\rho_{\text{calcd}}/\text{cm}^3$	2.405	2.405
μ/mm^{-1}	8.539	8.541
<i>F</i> (000)	1456.0	1456.0
Crystal size/mm ³	0.2 × 0.15 × 0.1	0.2 × 0.15 × 0.1
Radiation	MoKα ($\lambda = 0.71073$)	MoKα ($\lambda = 0.71073$)
2θ range for data collection/°	4.34 to 52.884	4.338 to 53.05
Index ranges	-24 ≤ <i>h</i> ≤ 24, -9 ≤ <i>k</i> ≤ 9, -18 ≤ <i>l</i> ≤ 19	-24 ≤ <i>h</i> ≤ 24, -9 ≤ <i>k</i> ≤ 9, -19 ≤ <i>l</i> ≤ 19
Reflections collected	20995	18471
Independent reflections	4432 [$R_{\text{int}} = 0.0288$, $R_{\text{sigma}} = 0.0269$]	4450 [$R_{\text{int}} = 0.0277$, $R_{\text{sigma}} = 0.0287$]
Data/restraints/parameters	4432/1/219	4450/1/219
Goodness-of-fit on <i>F</i> ²	1.033	1.049
Final R indexes [$I \geq 2\sigma(I)$]	$R_1 = 0.0216$, $wR_2 = 0.0497$	$R_1 = 0.0222$, $wR_2 = 0.0515$
Final R indexes [all data]	$R_1 = 0.0241$, $wR_2 = 0.0504$	$R_1 = 0.0242$, $wR_2 = 0.0521$
Largest diff. peak/hole/eÅ ⁻³	0.86/-1.12	0.89/-1.08
Flack parameter	0.003(5)	0.021(5)
CCDC	2373620	2373939

Table S3. Cu-Cu distance (Å) for *R/S*-Cl and *R/S*-Br.

Compounds	<i>R</i> -Cl	<i>S</i> -Cl	<i>R</i> -Br	<i>S</i> -Br
Cu1-Cu2	2.828(3) Å	2.837(3) Å	2.7487(14) Å	2.842(3) Å
Cu1-Cu3	2.6214(19) Å	2.599(2) Å	2.5815(13) Å	2.6563(13) Å
Cu1-Cu4	2.6120(17) Å	2.6715(18) Å	2.6571(12) Å	2.5796(13) Å
Cu2-Cu3	2.6120(17) Å	2.6715(18) Å	2.6571(12) Å	2.5796(13) Å
Cu2-Cu4	2.6214(19) Å	2.599(2) Å	2.5815(13) Å	2.6563(13) Å
Cu3-Cu4	2.873(3) Å	2.772(3) Å	2.842(2) Å	2.7469(14) Å
Average	2.6946 Å	2.6917 Å	2.6768 Å	2.6780 Å

Table S4. Comparison of PL parameters for a typical zero-dimensional organic-inorganic copper (I) halide: emission wavelength (λ_{em}), PL lifetime (τ), and PLQY.

Chemical formula	Peak position	Lifetime	PLQY	Ref
<i>R</i> -Cl	666 nm	9.96 μs	46%	This work
<i>S</i> -Cl	666 nm	9.95 μs	45%	This work
<i>R</i> -Br	610 nm	13.3 μs	95%	This work
<i>S</i> -Br	610 nm	13.6 μs	96%	This work
(MBA) ₄ Cu ₄ I ₄ (MBA = methylbenzylammonium)	630 nm	15.4 μs	60%	¹
(DBA) ₄ Cu ₄ I ₄ (DBA = dibenzylamine)	584 nm	20.3 μs	94%	²
PEA ₄ Cu ₄ I ₄ (PEA = phenethylamine)	633 nm	13.0 μs	73%	³
(DIET) ₃ Cu ₃ Br ₃ (DIET = 1,3-diethyl-2-thiourea)	515 nm	0.60 μs	69%	⁴
(C ₁₉ H ₁₈ P) ₂ Cu ₄ I ₆	620 nm	2.10 μs	87%	⁵
(C ₈ H ₂₀ N) ₂ Cu ₂ Br ₄	468 nm	56.0 μs	99%	⁶
Cu ₄ I ₄ (<i>R/S</i> -3-quinuclidinol) ₃	575 nm	10.7 μs	100%	⁷
[Cu ₄ I ₄ (PPh ₂ (C ₆ H ₄ -CH ₂ OH)) ₄]·CH ₃ CN	542 nm	3.92 μs	73%	⁸

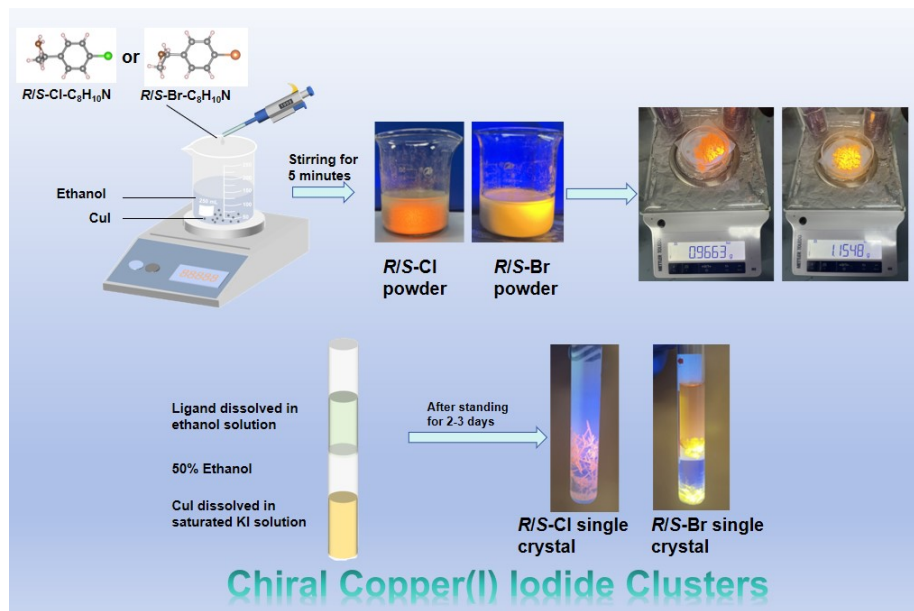


Figure S1. Schematic illustrations for the synthesis processes of *R/S*-Cl and *R/S*-Br powders and single crystals.

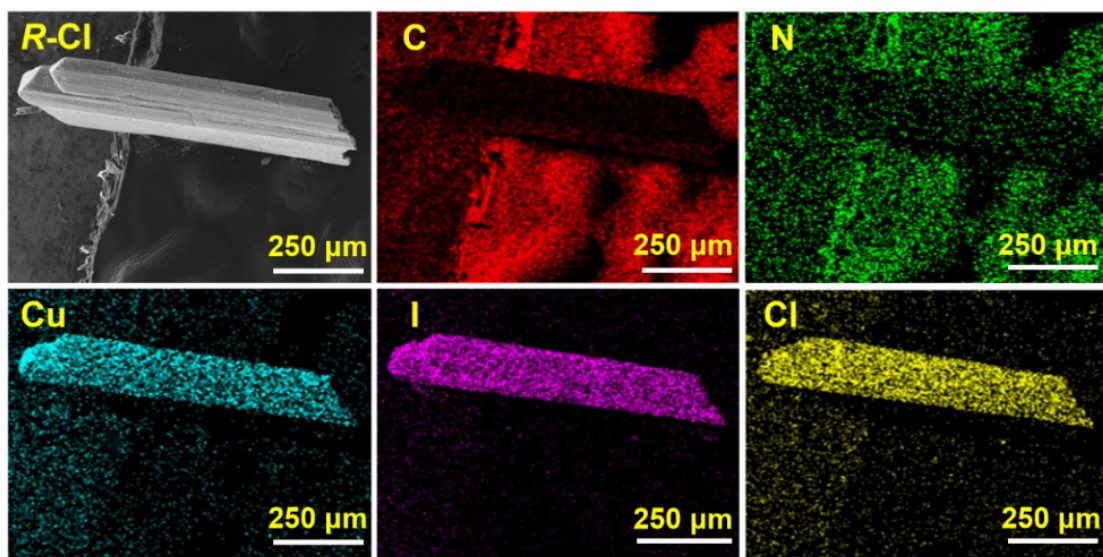


Figure S2. SEM image and EDS mappings of *R*-Cl SCs with the corresponding atomic maps.

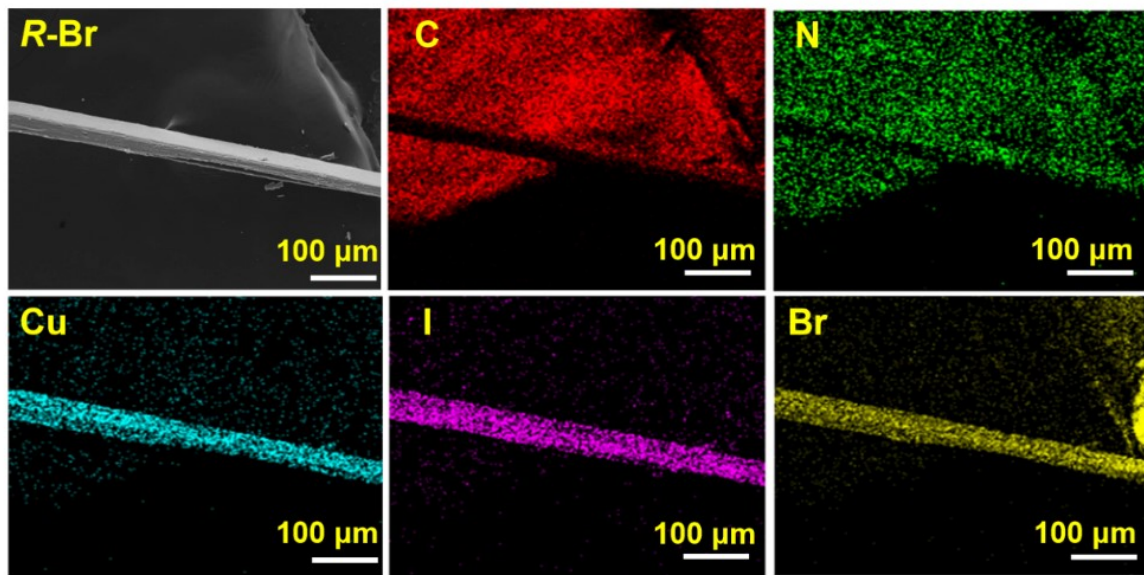


Figure S3. SEM image and EDS mappings of *R*-Br SCs with the corresponding atomic maps.

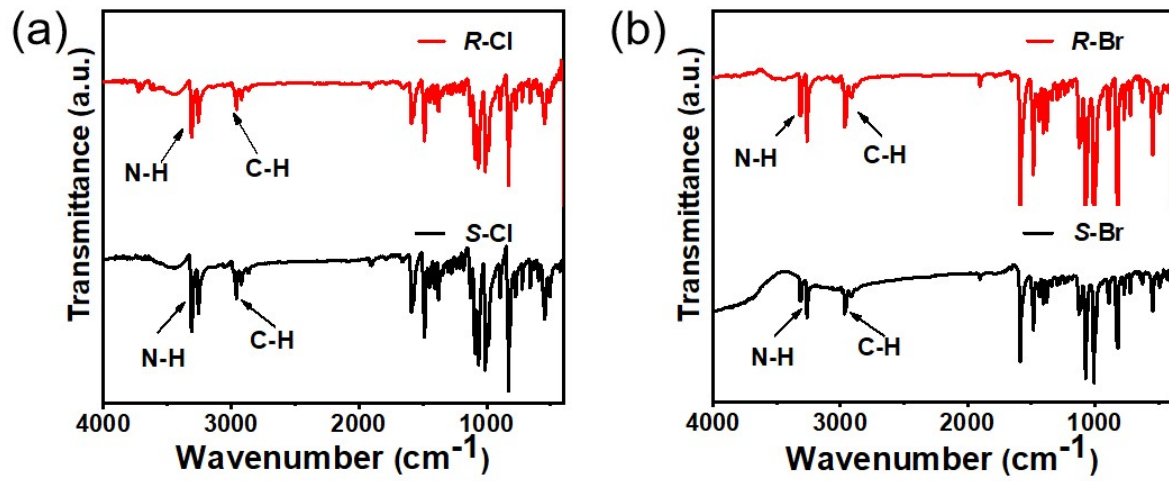


Figure S4. FTIR spectra of *R/S*-Cl (a) and *R/S*-Br (b).

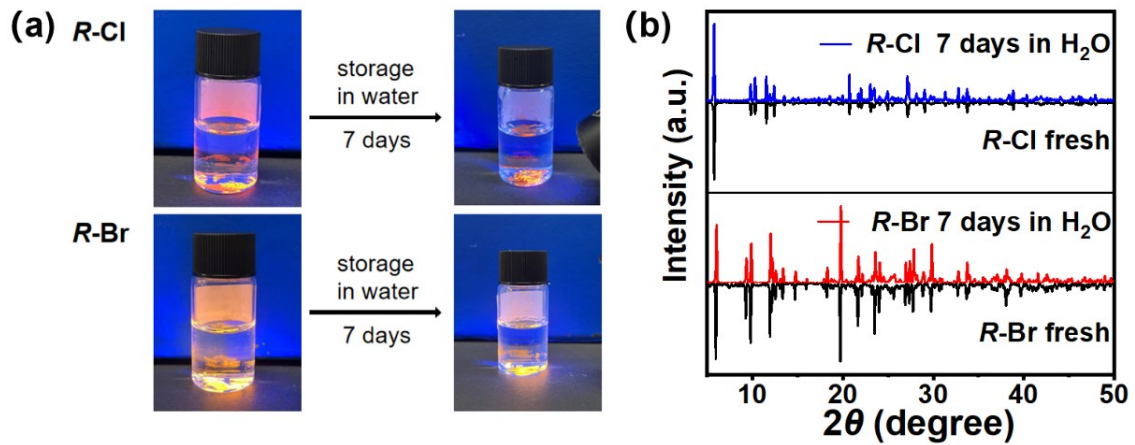


Figure S5. (a) Photographs of luminescence of *R*-Cl and *R*-Br before and after 7 days of storage in water. (b) XRD patterns of *R*-Cl and *R*-Br before and after stored in water for 7 days.

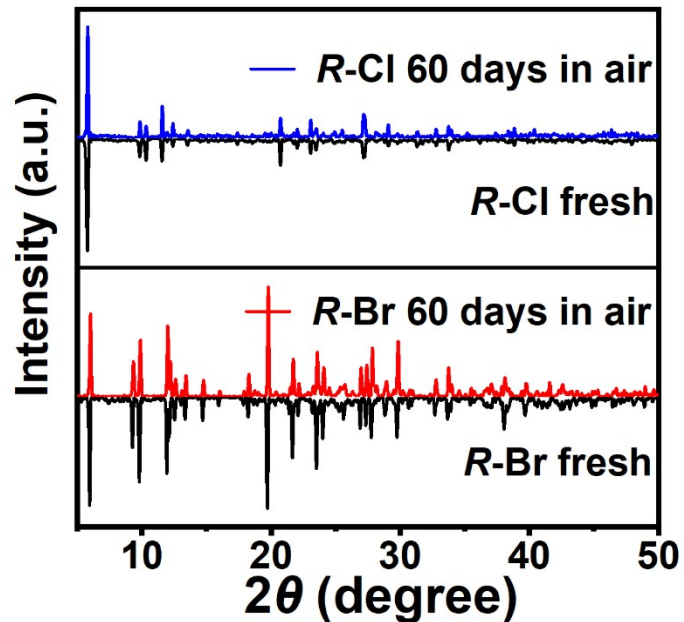


Figure S6. XRD patterns of *R*-Cl and *R*-Br before and after stored in air for 60 days.

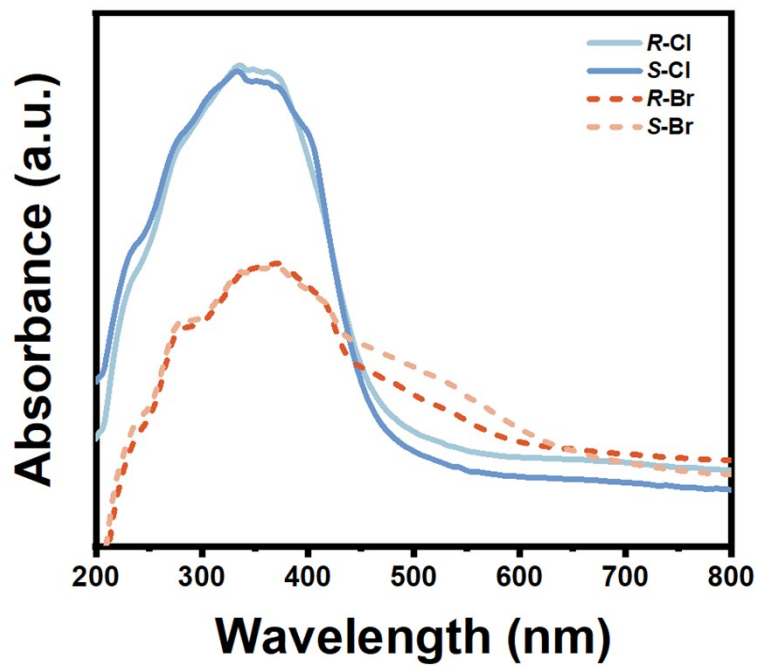


Figure S7. UV-vis absorption spectra of *R/S*-Cl and *R/S*-Br single crystals

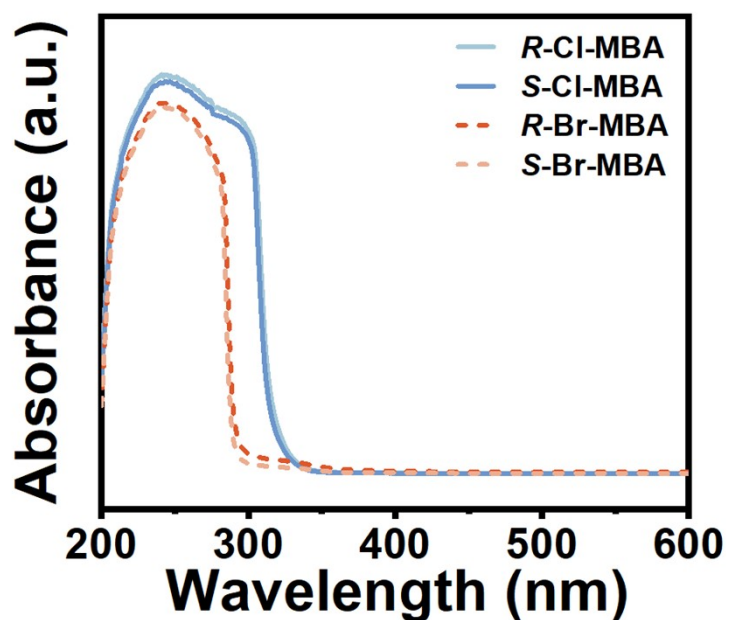


Figure S8. UV-vis absorption spectra of *R/S*-X-MBA ligand.

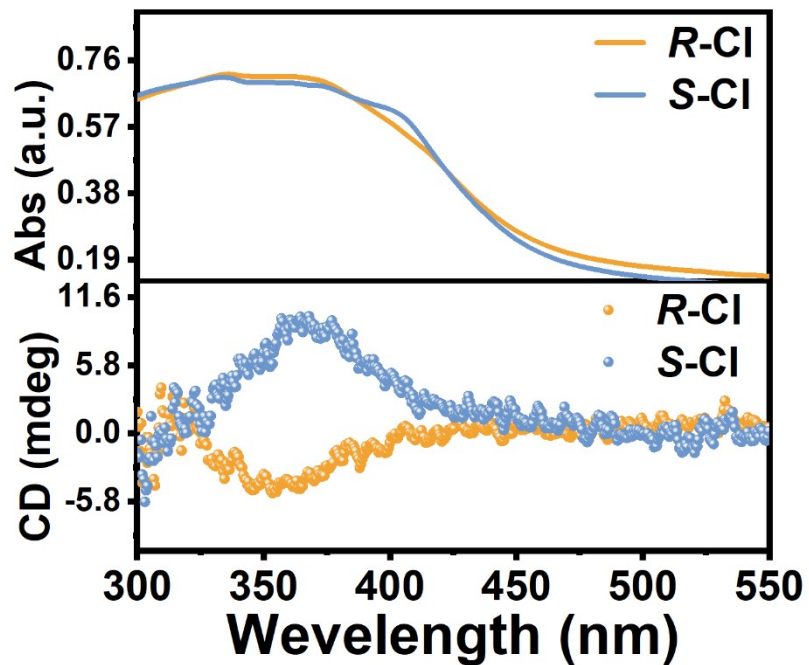


Figure S9. The CD and absorption spectra of *R/S*-Cl.

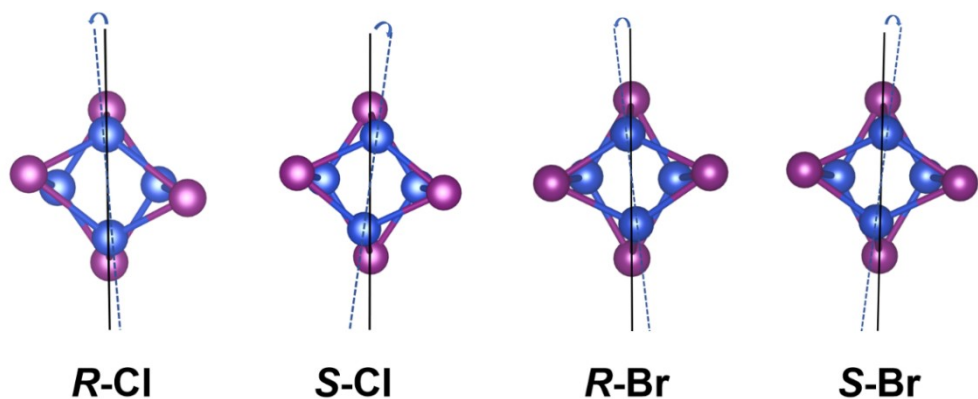


Figure S10. Cu_4I_4 framework of the *R/S*-Cl and *R/S*-Br enantiomeric pairs. The arrows represent their clockwise or counterclockwise twisting directions.

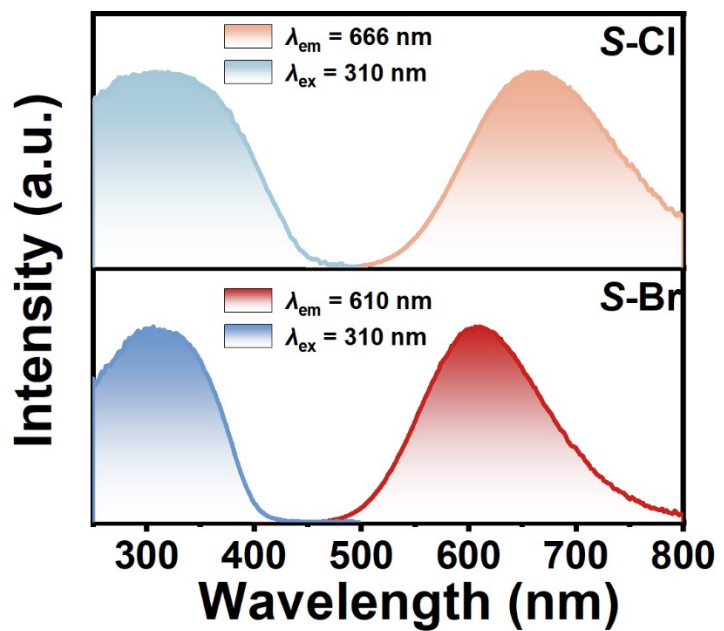


Figure S11. PLE and PL spectra for *S*-Cl and *S*-Br single crystals at room temperature.

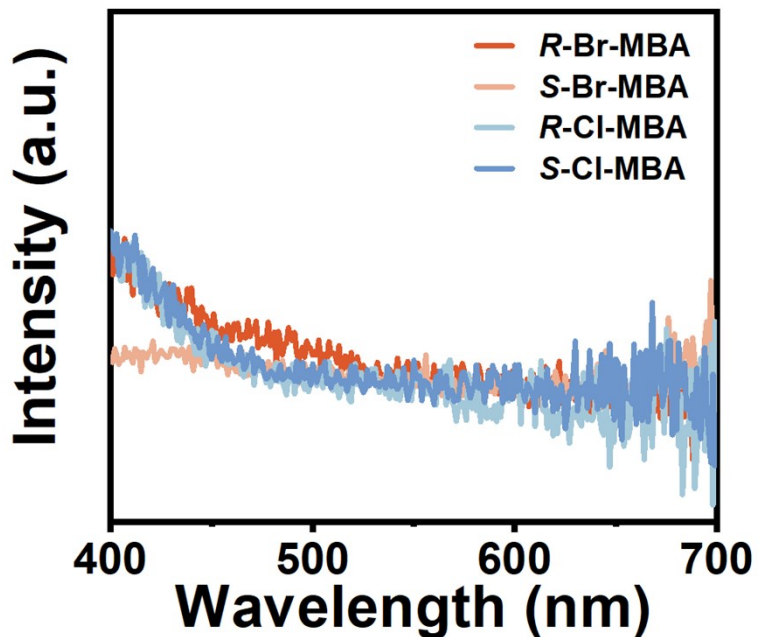


Figure S12. PL spectra for *R/S*-X-MBA ligand at room temperature.

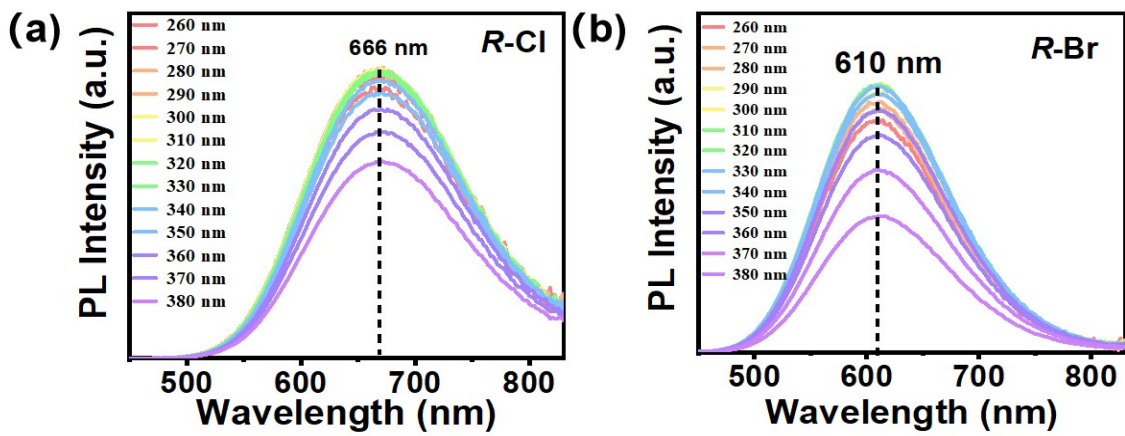


Figure S13. (a-b) PL spectra achieved by *R*-Cl and *R*-Br with different excitation wavelengths.

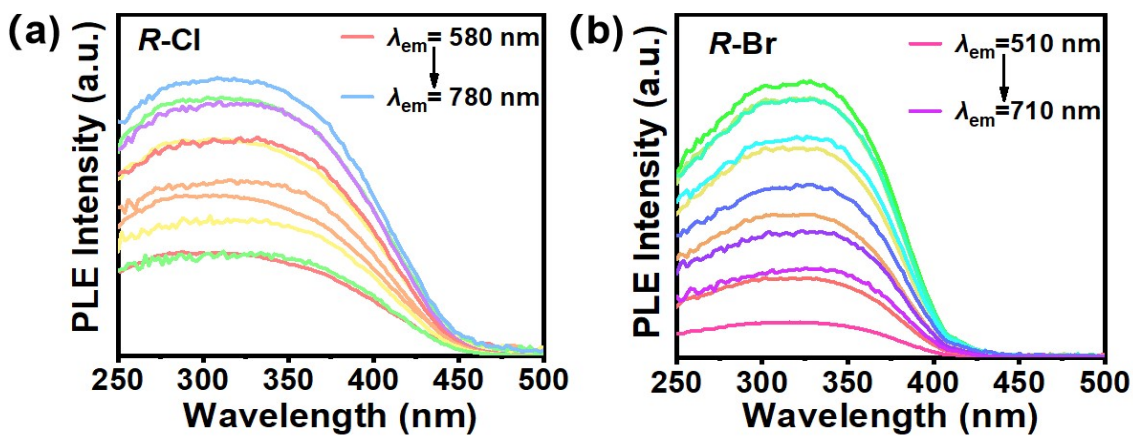


Figure S14. (a-b) PL excitation spectra of *R*-Cl and *R*-Br crystals by emission at different wavelengths.

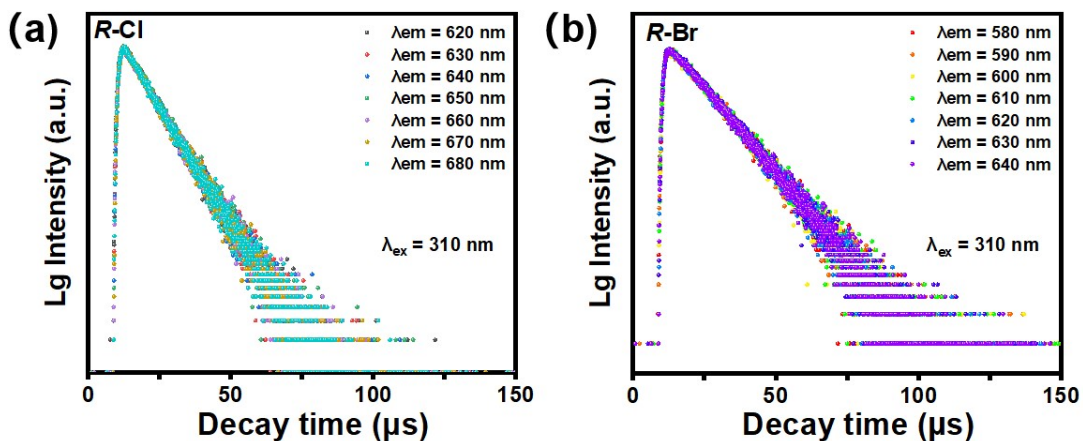


Figure S15. (a-b) Emission wavelength dependent TRPL decay curves of *R*-Cl and *R*-Br.

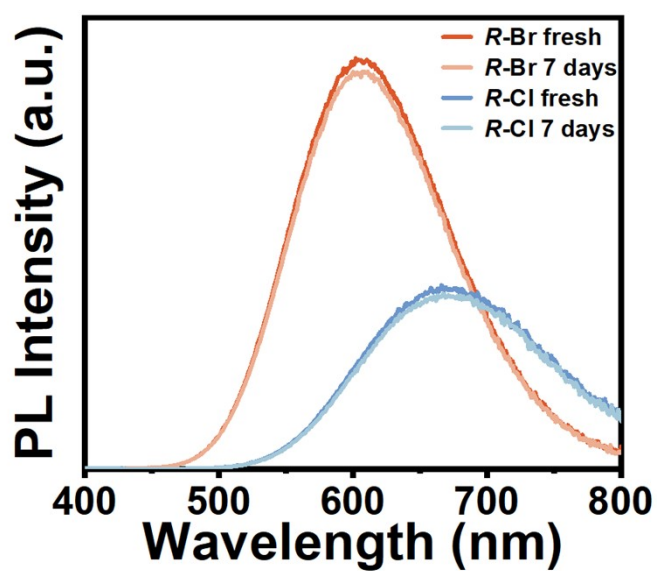


Figure S16. (a) PL spectra of *R*-Cl and *R*-Br after being stored in water for 7 days.

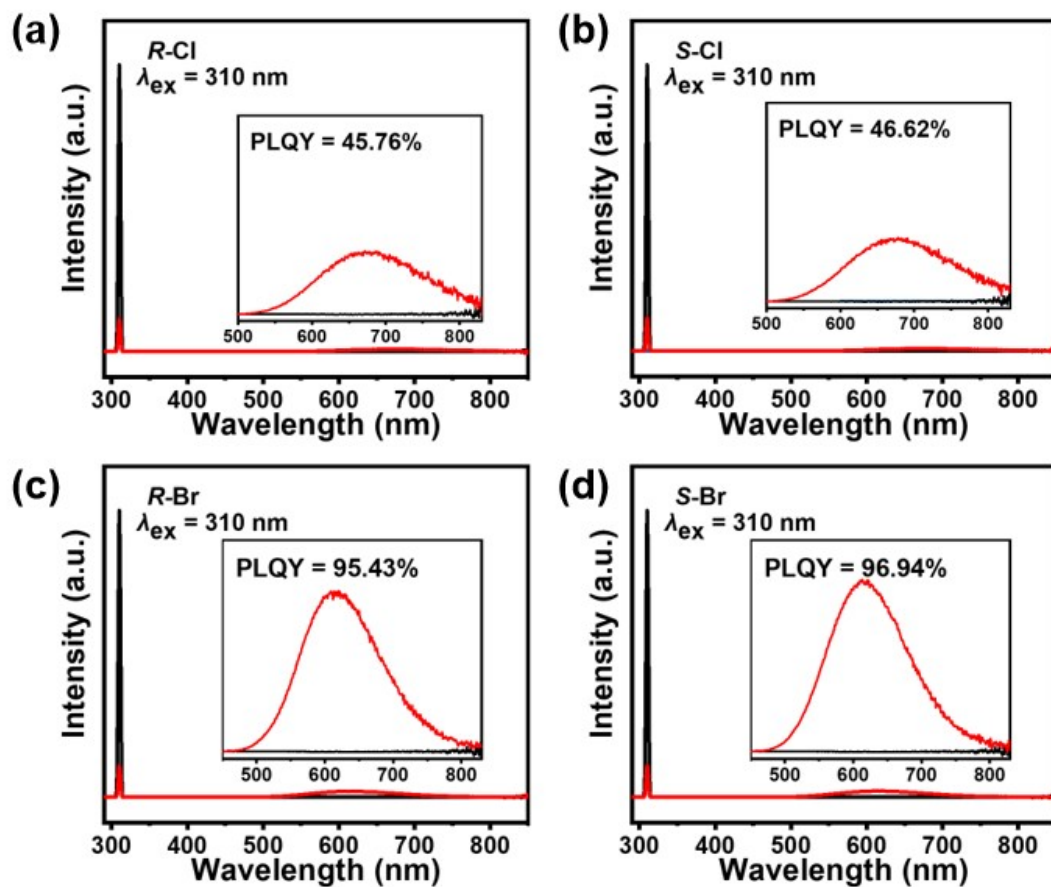


Figure S17. PLQY of *R/S*-Cl (a-b) and *R/S*-Br (c-d).

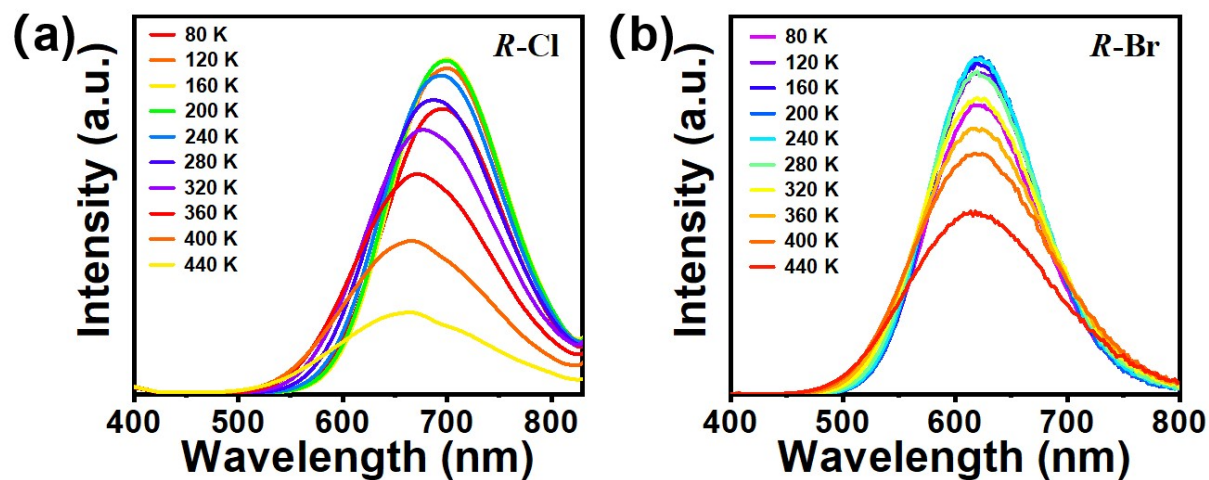


Figure S18. Temperature-dependent PL curves ($\lambda_{\text{ex}} = 310$ nm) of *R*-Cl (a) and *R*-Br (b) single crystals.

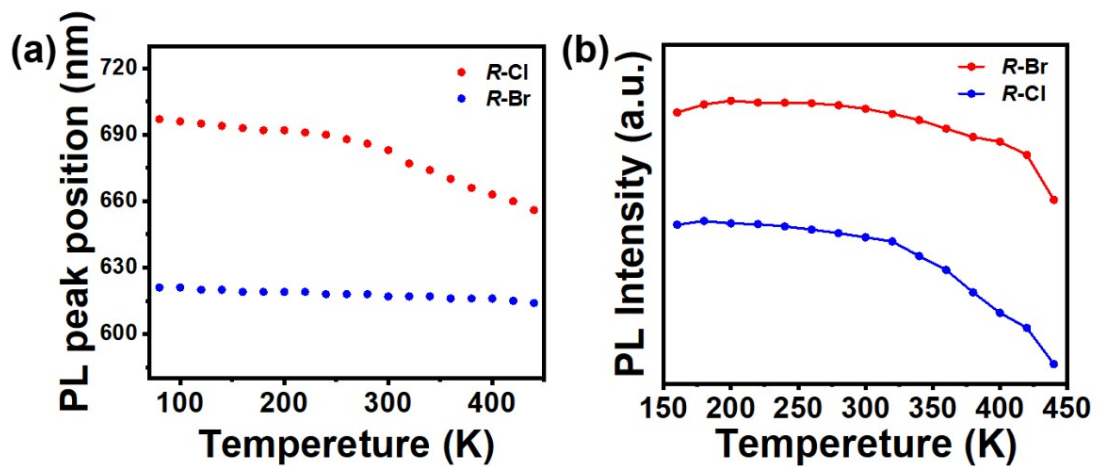


Figure S19. (a) Temperature-dependent PL peak position of *R*-Cl and *R*-Br. (b) Temperature-dependent PL intensity of *R*-Cl and *R*-Br.

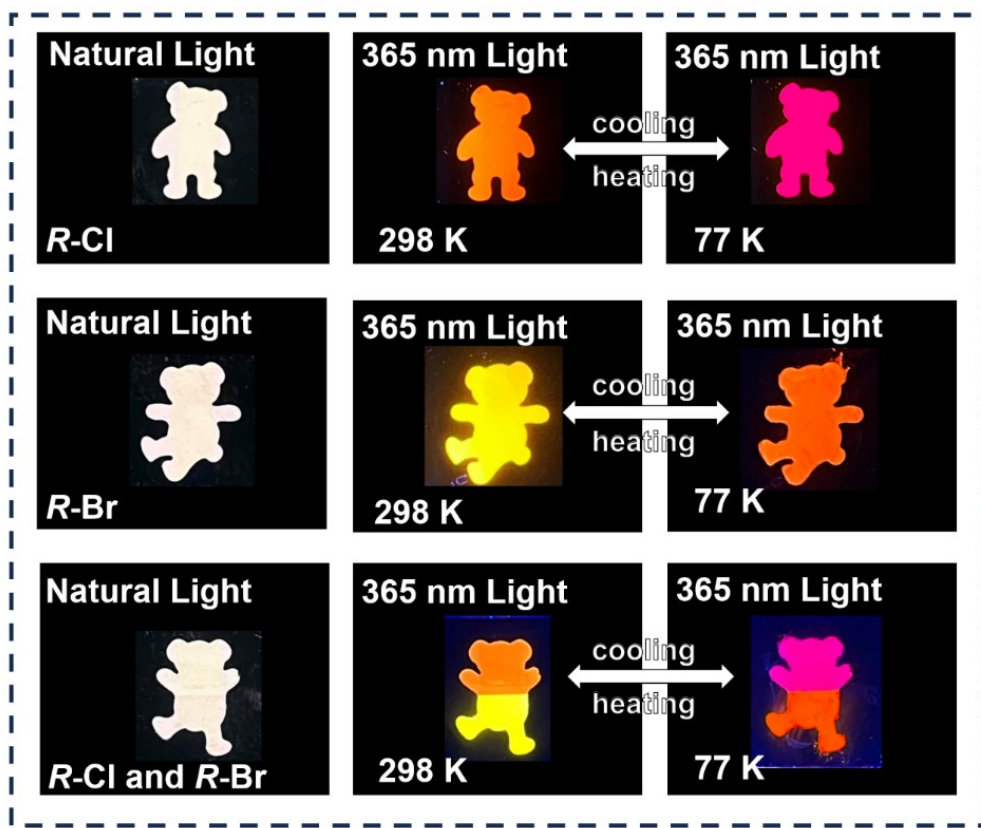


Figure S20. Visualization of *R*-Cl and *R*-Br luminescent color dependence on temperature.

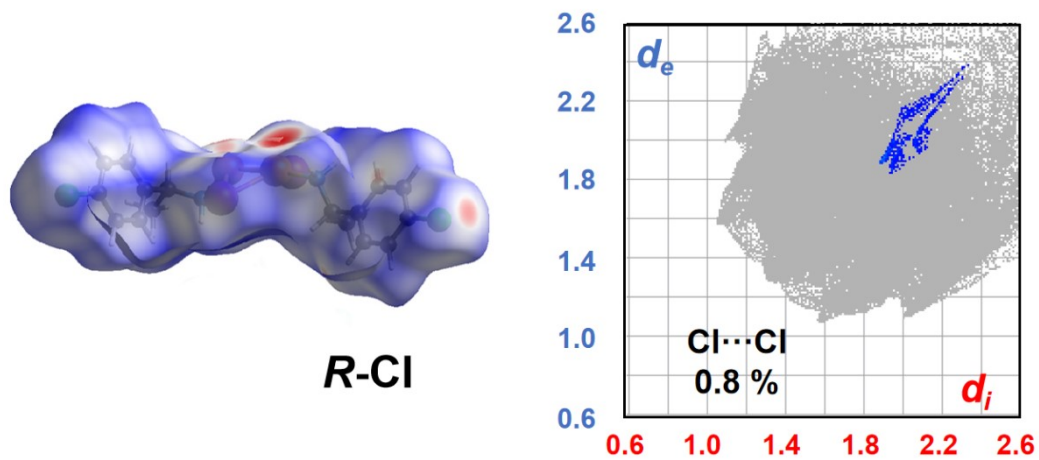


Figure S21. The hirshfeld surface of the organic cations and the 2D fingerprints of *R*-Cl.

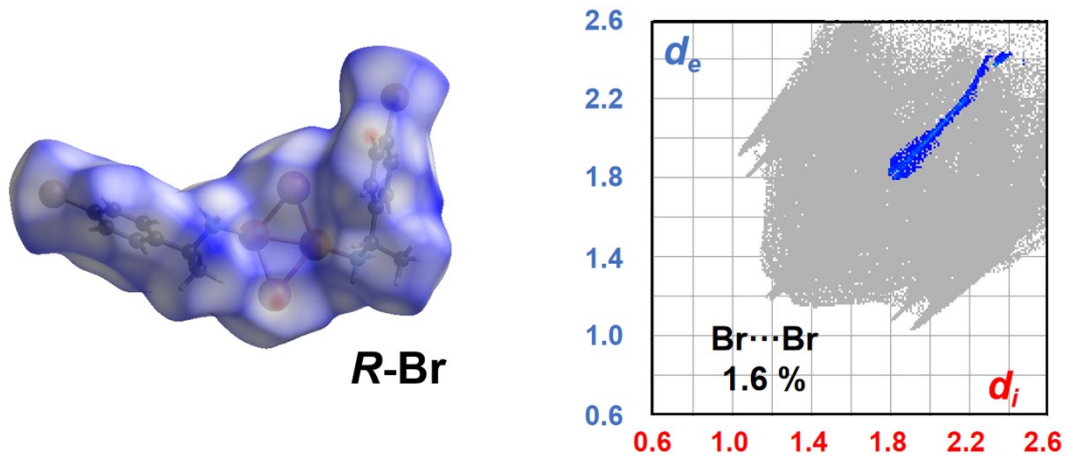


Figure S22. The hirshfeld surface of the organic cations and the 2D fingerprints of *R*-Br.

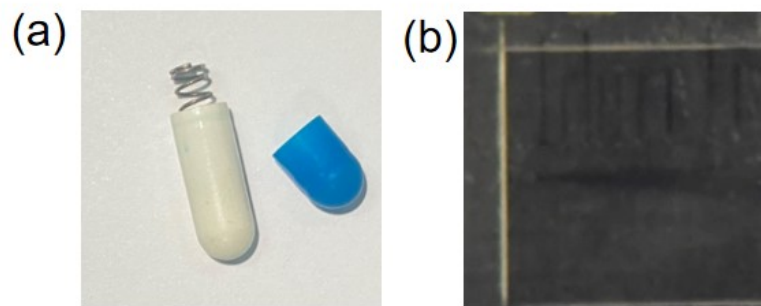


Figure S23. Photographs of springs (a) and scales (b) used for imaging.

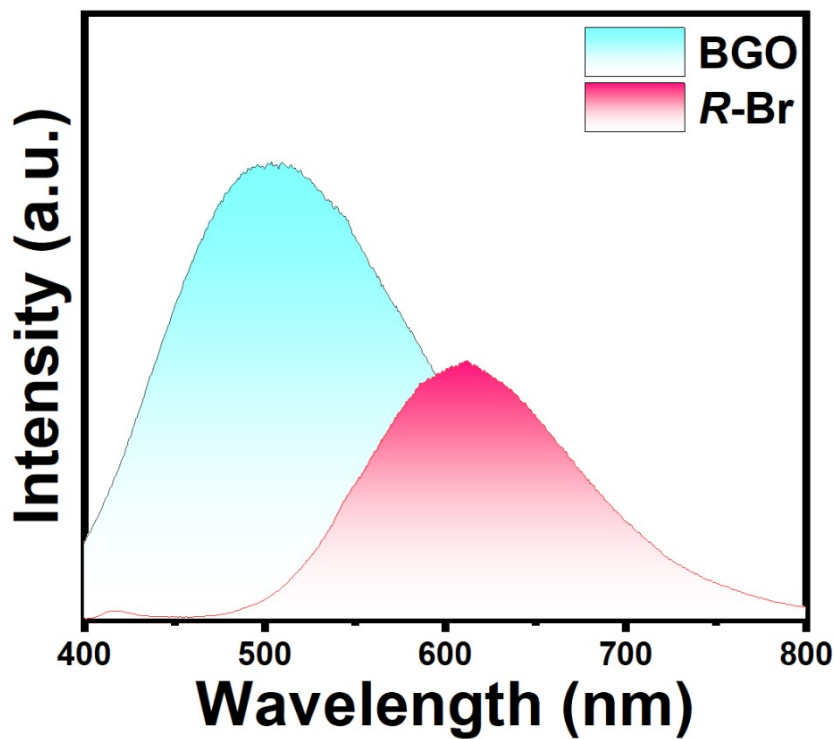


Figure S24. X-ray radioluminescence (RL) spectra of *R*-Br and $\text{Bi}_4\text{Ge}_3\text{O}_{12}$ (BGO) under X-ray irradiation.

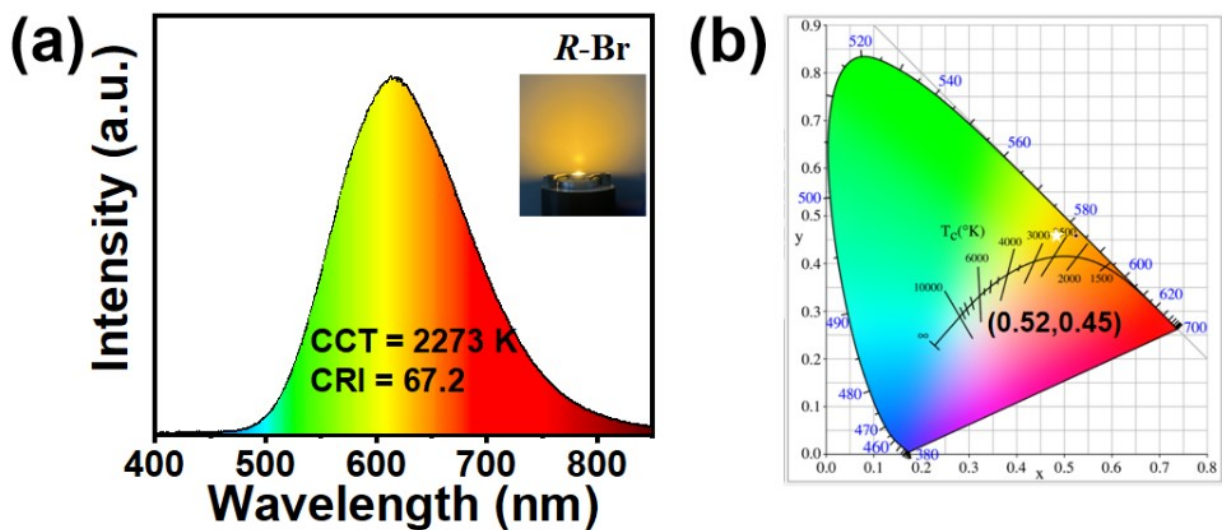


Figure S25. (a) Emission spectra of LED (the inset are photographs of the working device). (b) CIE chromaticity diagrams of LED.

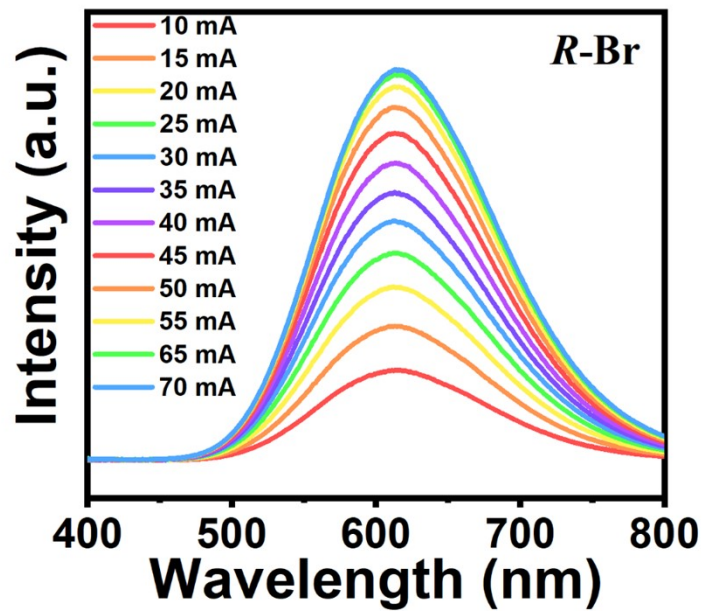


Figure S26. Variation of emission spectra with different currents of *R*-Br LEDs.

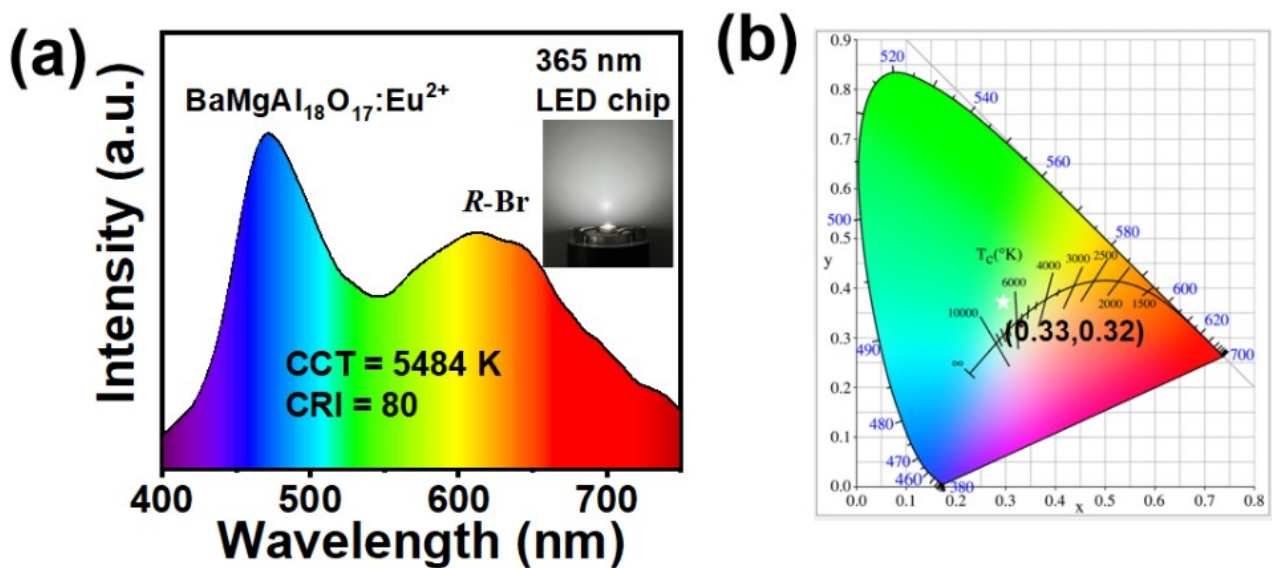


Figure S27. (a) Emission spectra of LED (the inset are photographs of the working device). (b) CIE chromaticity diagrams of LED.

References

- (1) Yao, L.; Niu, G.; Li, J.; *et al.* Circularly Polarized Luminescence from Chiral Tetranuclear Copper(I) Iodide Clusters. *The Journal of Physical Chemistry Letters* **2020**, *11* (4), 1255-1260.
- (2) Hu, Q.; Zhang, C.; Wu, X.; *et al.* Highly Effective Hybrid Copper(I) Iodide Cluster Emitter with Negative Thermal Quenched Phosphorescence for X-Ray Imaging. *Angewandte Chemie International Edition* **2023**, *62* (11), e202217784.
- (3) Fang, S.; Li, H.; Xie, Y.; *et al.* Zero-Dimensional Organic-Inorganic Hybrid Copper-Based Halides with Highly Efficient Orange-Red Emission. *Small* **2021**, *17* (42), 2103831.
- (4) Han, K.; Jin, J.; Su, B.; *et al.* Promoting Single Channel Photon Emission in Copper(I) Halide Clusters for X-Ray Detection. *Advanced Optical Materials* **2022**, *10* (20), 2200865.
- (5) Xie, L.; Liu, Z.; Yang, H.; *et al.* Ultra Broad-Band Excitable Organic-Inorganic Copper(I) Halides: Large-Scale Synthesis, Outstanding Stability, and Highly Efficient White Light-Emitting Diodes Application. *Advanced Optical Materials* **2024**, *12*, 2401050.
- (6) Su, B.; Jin, J.; Han, K.; *et al.* Ceramic Wafer Scintillation Screen by Utilizing near-Unity Blue-Emitting Lead-Free Metal Halide $(C_8H_{20}N)_2Cu_2Br_4$. *Advanced Functional Materials* **2023**, *33* (5), 2210735.
- (7) Chen, J.; Pan, X.; Zhang, X.; *et al.* One-Dimensional Chiral Copper Iodide Chain-Like Structure $Cu_4I_4(R/S\text{-}3\text{-Quinuclidinol})_3$ with near-Unity Photoluminescence Quantum Yield and Efficient Circularly Polarized Luminescence. *Small* **2023**, *19* (25), 2300938.
- (8) Utrera-Melero, R.; Huitorel, B.; Cordier, M.; *et al.* Combining Theory and Experiment to Get Insight into the Amorphous Phase of Luminescent Mechanochromic Copper Iodide Clusters. *Inorganic Chemistry* **2020**, *59* (18), 13607-13620.